Flame-vortex interaction : effect of residence time and formulation of a new efficiency function

F. Thiesset[a], G. Maurice[a,b], F. Halter[*a], N. Mazellier[b], C. Chauveau[a], I. Gökalp[a]

[a] *CNRS ICARE, Avenue de la Recherche Scientifique, 45072 Orléans Cedex 2 France*
[b] *University of Orléans, INSA de Bourges, PRISME, EA 4229, 45072 Orléans, France*

Abstract

In this study, a combined experimental and numerical investigation of a toroidal vortex interacting with a stagnation premixed flame is carried out with the aim of quantifying the ability of such a vortex to stretch the flame. It was found that, although inferred from exactly similar numerical simulations, available parametric expressions for the efficiency function (the ratio of the flame stretch to vortex strain) do not agree in the way the latter should behave when the ratio of the vortex rotational velocity U_θ to the laminar flame speed S_L is increased and that they are unequally accurate when compared to experimental data. Moreover, none of them can describe the non monotonic evolution of the efficiency function with U_θ/S_L which is observed in both experimental data and numerical simulations of a 'isothermal' propagating interface. In addition, whilst previous studies have focused only on the impact of U_θ/S_L and R_v/δ_L (R_v being the vortex typical size and δ_L the laminar flame thickness) our study reveals the importance of other parameters, the most important of which being the residence time of the vortex associated with its convection velocity. These results yield a new formulation for the efficiency function which compares favourably well with experimental data.

Keywords: Flame vortex interactions, Efficiency function, Stagnation premixed flames

1. Introduction

Understanding and predicting the different mechanisms at play in turbulent premixed flames is a tremendously difficult challenge. The main reasons for that is that there is still a lack of knowledge of the structural mechanics of the turbulent flow field itself which reveals a large variety of turbulent scales. A given eddy thus experiences many different processes induced by turbulent scales of different sizes, such as vortex stretching, vortex sweeping, production of kinetic energy by local velocity gradients, diffusion by viscosity, these effects being particularly arduous to model. In addition, when reacting flows are concerned, the flame does not act as a passive scalar because of its propagative character and the inherent heat release that locally modifies the fluid physical properties and counteracts on the fluid motion. The high local flame curvature and strain, also impact its local consumption or displacement speed in a way which remains poorly understood.

There is thus a need for prior fundamental investigations of the interactions between the fluid motion and a flame in simplified and well controlled situations. One of these is the case of a flame interacting with a single vortex dipole. Pioneer studies of Flame-Vortex Interactions (hereafter abbreviated by FVI) emerged in the 90's with notably Poinsot et al. [1], Roberts and Driscoll [2], Wu and Driscoll [3], Roberts et al. [4], Lee and Santavicca [5] and more recently with Colin et al. [6], Charlette et al. [7], Bougrine et al. [8].

Although (and maybe thankfully) some effects such as vortex stretching are not present, FVI remain archetypal of the processes at play in real turbulent flames. The aforementioned investigations on FVI have led notably to the construction of the so-called spectral diagrams which allows to identify the conditions needed for a vortex to stretch the flame, to create pockets of fresh gas or to locally quench the flame. In addition, these results had allowed to provide efficiency functions, i.e. the transfer function between vortex strain and flame stretch. In this prospect, Colin et al. [6], Charlette et al. [7] have focused on the effect of vortex size R_v relative the flame thickness δ_L and vortex rotational velocity U_θ relative to flame speed S_L. More recently, the effect of Lewis number has been incorporated by Bougrine et al. [8]. These efficiency functions are extremely valuable as they are widely used in LES of turbulent premixed combustion in order to model the sub-grid scale wrinkling factor [6, 7, 8].

The aim of the present study is to explore one par-

*Corresponding author at: CNRS ICARE, Avenue de la Recherche Scientifique, 45072 Orléans Cedex 2 France
Email: fabien.halter@cnrs-orleans.fr (F. Halter)

ticular aspect of the interaction between the flow motion and a flame, which we referred to as the *strain-sweeping competition* (see for instance the review by Driscoll [9]). This competition can be conceptually described in terms of time-scales. A given scale r with characteristic velocity u_r has a strain characteristic time scale τ_s given by the Kolmogorov theory [10] $\tau_s \propto r/u_r \propto r^{2/3}$. Previous studies devoted to FVI investigations [1, 2, 3, 4, 5, 6, 7, 8] indicate that the smaller this time scale, the larger is the flame stretch. On the other hand, Tennekes [11] suggested that another relevant time scale in a turbulent flow is the convection time scale. He pointed out that a given scale of size r is convected by the large scales, i.e. with characteristic velocity of the order of u', the root-mean-square of the velocity fluctuations. The sweeping time scale as called by [11] thus writes $\tau_c \propto r/u'$. This has been verified experimentally by e.g. Poulain et al. [12]. In the field of combustion the sweeping time scale is generally referred to as the residence time [9] and basically describes the duration of the interaction of a vortex located in the vicinity of the flame. As far as the sweeping (or residence) time scale is concerned, FVI [2, 3] corroborates the intuitive statement that the smaller this time scale, the smaller the flame stretch. In turbulent flames, there is thus a competition between turbulent strain and turbulent convection, the latter phenomenon acts in decreasing the flame stretch whereas the former has the opposite effect. It is thus worth investigating these effects independently in order to give further insight into their respective influence on the flame. Further, a more complete expression for the efficiency function which accounts for both strain and sweeping effects could be derived and used in LES.

In the present study, a new experimental set-up was designed in the goal of quantifying the degree of the interactions between a vortex dipole and a stagnation premixed flame. Some simple numerical simulations based on the 'isothermal' G-equation, have been further carried out and validated against experimental data. Such simulations allow to assess the effect of the convection velocity and rotational velocity independently. Finally, the respective effect of these two phenomena on flame stretch are separately quantified are incorporated into a more complete expression for the efficiency function.

2. Experimental apparatus

Investigations are carried out in a single jet stagnation flame configuration which is a modified version of that used by Bouvet et al. [13]. A schematic of the burner is provided in Fig. 1. A laminar strained flame is stabilized against a 4-mm-thick stainless steel plate. The stagnation plate is attached to an alumina foam plug selected for its insulating properties. The fuel and oxidizer are first introduced through the side of the burner. A so-called 'particle diffuser cone' filled with 6 mm glass beads is used to ensure a homogeneous mixture in the nozzle plenum. The reactive

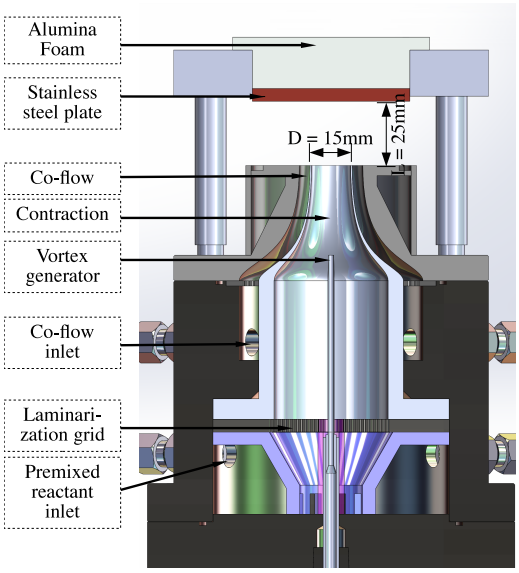

Figure 1: Schematic of the experimental setup

mixture then flows into the burner plenum through a 5 mm thick aluminium grid. It is finally accelerated in the converging section with a $D = 15$mm outflow diameter, creating an upward-oriented jet with a top hat velocity profile. The burner-to-stagnation plate distance L was fixed to 25mm, given a L/D ratio greater than unity as generally recommended. Moreover, it allows to stabilize flames sufficiently far from the plate to track the flame/vortex interaction without being affected by the plate. To avoid external perturbations and improve flame stability, a laminar coaxial shroud of nitrogen is used. The nitrogen flow rate was set so that the coflow exit velocity closely matches the one of the main flow. In the present study, the wall stagnation configuration is preferred over the classical opposed jet configuration for the following reasons: *(i)* the experimental apparatus can be implemented and controlled easily (no need for upper burner) and *(ii)* wall-stabilized flames are generally found to be more stable than counterflow ones.

The flame front is tracked by means of Mie scattering laser tomography. For this purpose, use is made of a continuous Coherent Verdi G20 Laser which delivers up to 20W at 532nm. The light scattered by the particles is then captured by a Phantom V1210 camera, equipped with a 105mm F2.8 lens, working at an acquisition rate of 23005Hz with a field of view of 704×640 pixels^2 and the resolution was 0.038 mm/px. In both case, seeding of the flow is made by silicon droplets supplied by an atomizer. Typical size of droplets is about 1μm. It was checked that the flame height did not vary when the seeding was turned off suggesting that the laminar flame speed was not altered by the addition of silicon droplets in the flow.

The flame contour is then extracted as follows. Firstly, a contrast-limited adaptive histogram equal-

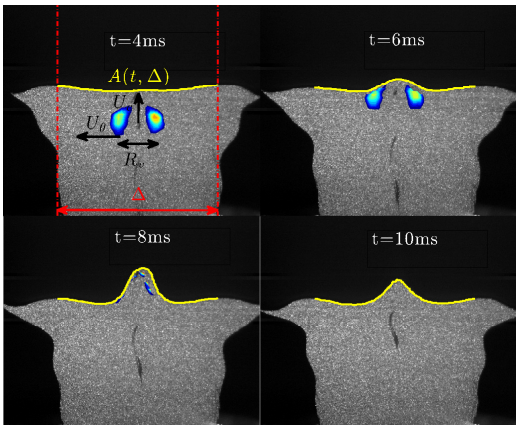

Figure 2: Time sequence of Mie scattering images of a typical FVI ($U_\theta/S_L = 1.43$). The flame contours and vorticity field are superimposed. The top of each image has been cropped to show only the first 20mm. The yellow line corresponds to the flame contours with area $A(t,\Delta)$ estimated over a domain of width Δ. U_θ, U_c are the vortex rotational and convection respectively, whilst R_v is the vortex core-to-core distance.

ization (CLAHE) is applied to the original images in order to optimize the contrast in the images. Then, to limit the pixelization associated with the CLAHE, images are filtered using a Gaussian filter of size equal to 4 times the spatial resolution. For the binarizing procedure, we use a standard threshold-based technique. More precisely, the histogram of the gray scale is calculated. The latter reveals two distinct peaks corresponding to the fresh and burned gas respectively. The threshold value for discriminating the flame contour is set as the average value between the gray scale of these two peaks. Yields estimations for the progress variable, noted c, which is by definition 0 and 1 in the unburned and burned gas respectively. The velocity field within the unburned mixture is estimated by classical Particle Image Velocimetry (PIV). For this purpose, the Matlab subroutines of Thielicke and Stamhuis [14] were used. A time sequence of Mie scattering images at four distinct instants is shown in Fig. 2. The vorticity field and flame contours are superimposed. The time $t_0 = 0$ was set arbitrarily as the time t where the vortex center was 5mm downstream the burner outlet. One observes that at a time t=4ms, the flame is rather flat suggesting that the vortex generator is sufficiently far from the burner outlet for not creating a wake. As the vortex is convected (t=6ms ad 8ms), the flame is increasingly stretched. Its area then reaches a maximum before decreasing (t=10ms) while the flame goes back to its original position.

Three equivalence ratios for the reactive mixture $\phi = 1, 0.9, 0.8$ have been considered. The laminar flame speed and thickness have been evaluated using the GRI-mech 3.0 mechanism together with the stagnation flame module of the CHEMKIN Pro software. The temperature of the wall, measured by Bouvet et al. [13], and was set to $800K$. It was found that $S_L = 40.3, 36.5, 30.6\text{cm.s}^{-1}$ and $\delta_L = 433, 463, 525\mu$m respectively for $\phi = 1, 0.9$ and 0.8. The strain rate was respectively 90, 86 and 77s^{-1} for $\phi = 1, 0.9$ and 0.8.

The toroidal vortex is generated by applying a pressure discharge of reactive mixture of same equivalence ratio than the main flow in a tube of 2mm diameter located on the centerline of the flow and 35mm upstream the burner outlet (Fig. 1). The discharge, of duration $\approx 10\mu$s, is controlled by two electro-valves connected by series. The intensity of the vortex is controlled by varying the pressure magnitude (with a precision of 1 Pa) within a pressurized tank located just upstream the two aforementioned valves.

For assessing the vortex parameters, i.e. the circumferential velocity U_θ, the convection U_c and the core-to-core distance R_v, the velocity field inferred from PIV was fitted by means of a Oseen vortex. Our experimental set-up allows to cover the range $0.5 \lesssim U_\theta/S_L \lesssim 2.5$ whereas R_v/δ_L slightly varies around 6.5. Our database thus lies between the no-effect limit and the quenching limit assessed by Roberts et al. [4].

3. Experimental results

3.1. Domain size effects

The focus of this paper is on the flame stretch associated with the interaction with a vortex. Given the vortex rotational velocity U_θ and the distance between vortex cores R_v (see Fig. 2), the vortex strain is generally estimated as U_θ/R_v [6, 7, 8]. On the other hand, the flame stretch is evaluated as

$$K(t,\Delta) = \frac{1}{A(t,\Delta)}\frac{\partial A(t,\Delta)}{\partial t} \tag{1}$$

where $A(t,\Delta) = \int y(s)\sqrt{x'^2 + y'^2}ds$ is the flame area at a time t evaluated over a domain of width Δ (see Fig. 2). s is the curvilinear parameter, y and x are the flame contour spatial coordinates and the prime denotes derivatives with respect to s. Then the efficiency function is defined as in [6, 7, 8], viz. $C(\Delta) = K_{\max}(\Delta)/(U_\theta/R_v)$, where $K_{\max}(\Delta)$ is the maximum value of $K(t,\Delta)$. The appearance of Δ in the efficiency function is new. In previous studies [6, 7, 8] a given value for $\Delta \approx 3R_v$ which corresponds to their simulation domain was chosen. However, it appears straightforward that $K_{\max}$ depends on Δ. Indeed, because the portion of flame interacting with the vortex is constant (i.e. there exists a Δ above which $\partial A/\partial t$ is independent of Δ), we expect $K_{\max}$ to decrease with Δ since $A(t,\Delta)$ continuously increases with Δ. Figure 3 presents the evolution of $K_{\max}$ with respect to Δ. It clearly appears that $K_{\max}$ rapidly decreases with respect to Δ and for Δ sufficiently large (i.e. for Δ larger to a certain Δ_i), it is found that $K_{\max}$ follows the relation

$$K_{\max} = K^0_{\max}\left[\frac{\Delta_i - \Delta_0}{\Delta - \Delta_0}\right]^2. \tag{2}$$

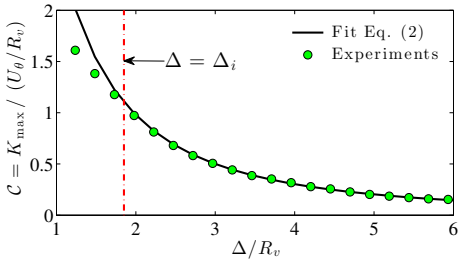

Figure 3: Evolution of $K_{\max}$ with Δ for $U_\theta/S_L = 1.43$. Symbols represent experimental data whilst the black line corresponds to the fit using Eq. (2). Also displayed in the vertical red line corresponding to the domain width $\Delta = \Delta_i$ above which Eq. (2) is valid

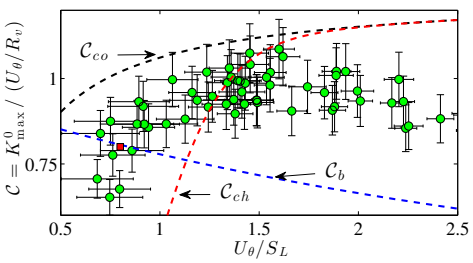

Figure 4: Efficiency function $C = K^0_{\max}/(U_\theta/R_v)$ as a function of U_θ/S_L. The black, red and blue dashed lines correspond respectively to the parametric expressions provided by Colin et al. [6], Charlette et al. [7], Bougrine et al. [8], corrected using Eq. (2) to obtain $K^0_{\max}$. Green circles correspond to the present measurements whilst the red square is taken from Bougrine et al. [8]

In Eq. (2), Δ_i represents the domain width above which $\partial A/\partial t$ is constant and Δ_0 is interpreted as a virtual origin, i.e. $K^{-1}_{\max} \to 0$ when $\Delta \to \Delta_0$. From our experimental database, it was found that Δ_i/R_v Δ_0/R_v were constant and are equal to 2.5 ± 0.05 and -0.5 ± 0.1.

As a consequence, it is shown here that the values for the efficiency function that were previously provided notably by Colin et al. [6], Charlette et al. [7], Bougrine et al. [8] are arbitrary in that sense that they were inferred for a given value of Δ/R_v. If they had chosen a different value for the simulation domain, they would have obtained different values. Moreover, the no-effect limit assessed by Poinsot et al. [1] which "corresponds to vortices which induce a maximum modification of the total reaction rate of about 5 percent", is also arbitrary not only because of the 5% threshold but also because the integrated reaction rate over the simulation domain depends on Δ. On the contrary, Roberts et al. [4] have chosen a local quantity for assessing the no-limit boundary, which in their case corresponds to a "peak OH intensity of a segment less than 1% of that of the undisturbed flame" which thus appears much more relevant.

3.2. Impact of vortex intensity

We now turn our attention to the effect of the vortex strength on the flame stretch. Figure 4 depicts the evolution of $C^0 = K^0_{\max}/(U_\theta/R_v)$ as a function U_θ/S_L (hereafter the superscript ^{0} on C will be removed). Experimental results are also compared to the predictions provided by Colin et al. [6], Charlette et al. [7], Bougrine et al. [8] which are respectively noted C_{co}, C_{ch} and C_b. Their respective analytical expressions are not recalled here but the reader can refer to [6, 7, 8] for more details.

Experimental uncertainties have been estimated as follows. The precision of the subpixel interpolation of the PIV algorithm is generally about 0.05 pixel. The uncertainty on the velocity field is therefore constant and equals to about 0.04m.s^{-1} provided the resolution and sampling frequency of our images. The error on the estimation of R_v provided by fitting experimental data with an Oseen vortex was generally of about 4%. The uncertainty in the determination of $K_{\max}$ was supposed to be negligible by comparison with the errors on both U_θ and R_v since A is readily measurable.

A careful analysis of Fig. 4 first reveals that, although acceptable, some departures between experimental data and the predictions of either [6, 7, 8] can be observed. By comparison with experiments, the efficiency function of Colin et al. [6] appears to be the more appropriate. However, it is worth stressing that, although based on exactly similar simulations, available parametric expressions for C do not agree in the way the latter should behave with respect to U_θ/S_L. Indeed, Colin et al. [6], Charlette et al. [7] both predict an increasing tendency of C with respect to U_θ/S_L whereas C_b leads to the opposite trend.

Although scattered, our experimental data suggest that the evolution of C is non monotonic, i.e. C first increases before slightly decreases for U_θ/S_L larger than about 1.5. The decreasing tendency of C was also observed in the DNS of Bougrine et al. [8] when the vortex strength was enhanced from $U_\theta/S_L = 0.8$ to 8 (note that there is a nice agreement between our experiments and the DNS data of Bougrine et al. [8] for $U_\theta/S_L = 0.8$). This observation can be readily explained by recalling an intense vortex will create high local curvatures which act in decreasing the total stretch of the flame. In other words, increasing the vortex strength can be less efficient it terms of flame stretch since it leads to too high curvatures.

Roberts and Driscoll [2] was first to realize that the flame stretch is also driven by the convection velocity U_c of the vortex dipole. More precisely, they suggested that for a given U_θ, increasing U_c yields a smaller flame stretch because the residence time of the vortex in the vicinity of the flame decreases. This intuitive statement was further confirmed by Wu and Driscoll [3] on the basis of propagating surface numerical simulations. There is thus a need for incorporating these two opposed effects (convection vs

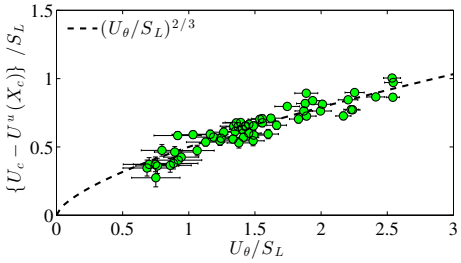

Figure 5: Convection velocity $U_c - U^u(X_c)$, where $U^u(X_c)$ is the streamwise velocity of the unperturbed flow at the vortex center location X_c, as a function of U_θ. The dotted line is a 2/3 power law.

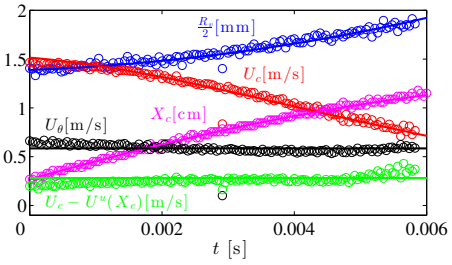

Figure 6: Time evolution of the vortex parameters for a given case in the database. Are represented the vortex core-to-core distance R_v (blue), the convection velocity U_c (red) and $U_c - U^u(X_c)$ (green), the vortex center streamwise position X_c, and the rotational velocity (black). Symbols are experimental data whilst lines stand for the simulation.

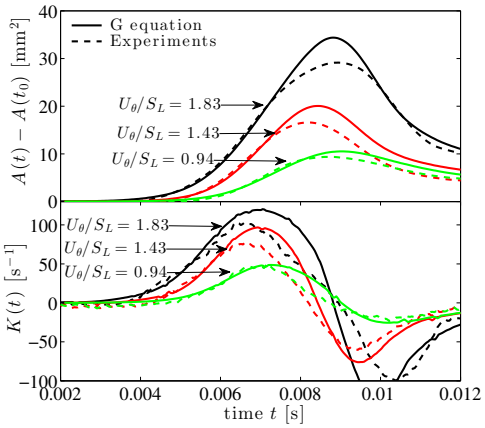

Figure 7: Time evolution of the flame area $A(t,\Delta)$ (a) and stretch $K(t,\Delta)$ (b) for Δ = 10mm, for three different ratio of U_θ/S_L = 0.94, 1.43, 1.83 (green, red and black respectively). Dashed and full lines correspond respectively to experimental and numerical data

rotational velocity) into a more complete expression of the efficiency functions. However, in our experiments, it was observed that increasing U_θ irremediably leaded to a higher convection velocity. It was found experimentally (Fig. 5) that the convection velocity $U_c - U^u(X_c)$ (U^u the streamwize velocity experienced by the vortex located at X_c) scales as $U_\theta^{2/3}$. Therefore, it is not possible from experiments to assess independently the respective influence of U_θ and U_c.

Consequently, following the lines of e.g. Wu and Driscoll [3] or Lee and Santavicca [5], we thus decided to perform simplified numerical simulations of the same burner in the goal of studying the effect of U_c and U_θ independently. These simulations consider the flame as a 'passive' propagating interface. Whilst such simulations neglect notably the heat release and the turbulence-chemistry interactions, they have the tremendous advantage of being extremely low-cost in terms of computational resources while keeping one of the most important aspect of turbulent flames, i.e. their propagative character.

4. Simulations of a vortex interacting with a propagating interface

4.1. Implementation and validation

Present numerical simulations consider the flame as a two-dimensional propagating interface convected by the fluid motion $\boldsymbol{U}$ while advancing at the laminar flame speed S_L. The kinematic relationship between the flame and the flow field is then given by the G-equation which writes

$$\frac{\partial G}{\partial t} + \boldsymbol{U}.\boldsymbol{\nabla} G = S_L|\boldsymbol{\nabla} G| \qquad (3)$$

In the present case, the velocity field is set as follows. First, U^u and V^u, i.e. the velocity component in the streamwise x and transverse y direction of unperturbed flow (before the generation of the vortex) is given by $U^u(x,y) = U_0 - 2\int a(x)dx$ and $V^u(x,y) = a(x) \times y$, where $U_0 = 1.23\text{m.s}^{-1}$ is the inlet velocity of the burner and $a(x) = \partial V^u/\partial y(y=0)$ is the transverse strain of the unperturbed flow. $a(x)$ was fitted from experiments using a second order polynomial. The coefficients of the polynomial were adjusted for each equivalence ratio.

Secondly, the vortex velocity field was added to U^u and V^u and set using the Oseen expression. The input parameters for the Oseen vortex are U_θ, X_c (the streamwize location of the vortex center) and R_v, the core-to-core distance. In the present case, by analyzing experimental data (see Fig. 6), it was found that U_θ does not vary with time and was therefore set to a constant. The vortex center X_c was convected at a velocity U_c, viz. $\partial X_c/\partial t = U_c$, where $U_c - U^u(X_c)$ was found to be constant (see Fig. 6). The time evolution of the vortex ring diameter R_v follows the relation [15] $R_v^{-1}\partial R_v/\partial t = a(X_c)$. In Fig. 6, the time evolution of vortex parameters issued from the experiments

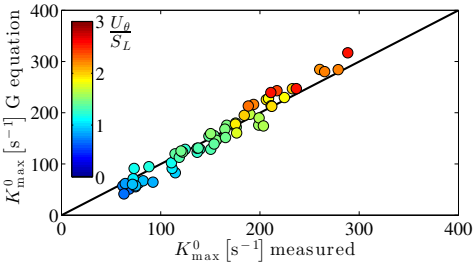

Figure 8: Maximum stretch $K^0_{\max}$ assessed by experiments versus $K^0_{\max}$ inferred from numerical simulations. Symbols are coloured by U_θ/S_L

are compared to that prescribed in the numerical simulations. All quantities compare extremely well and thus validate the procedure for establishing the velocity field.

The G-field was initialized as a signed distance with the iso-value $G = G_0 = 0$ located at the streamwise location x at which $U^u(x) = S_L$. Equation (3) is resolved using a third-order EN03 discretization scheme in space and 4th-order Runge-Kutta scheme for time advancement. The usual reinitialization procedure is also applied at each time step so that the G-field remains a signed distance. The mesh size is 500×500 corresponding to a domain size of 25×25mm^2. It was checked that increasing the mesh size up to 1000×1000 points yielded only marginal differences.

Numerical simulations have been validated against experimental data. Results for three different values of $U_\theta/S_L = 0.94, 1.43, 1.83$ are presented in Fig. 7. The increase of $A(t,\Delta)$ is very nicely reproduced by the simulation, whilst some slight departures are observed close to the maximum of $A(t,\Delta)$. This indicates that the early stage of the interaction (i.e. before the vortex reaches the burnt gas) relies mainly on a kinematic interaction and that the heat release does not play a significant role. The simulated flame stretch compares favourably well with experiments for the three cases represented in Fig. 7. A scatter plot of the measured vs simulated $K^0_{\max}$ for the entire database is further given in Fig. 8. Here again, a nice agreement is observed. Departures between numerical and experimental data for $K^0_{\max}$ lies within 20% on average.

4.2. Formulation of a new efficiency function

By use of such numerical simulation, the effect of U_c and U_θ on $K^0_{\max}$ can thus be studied independently with the aim of incorporating these parameters in a more complete expression for the efficiency function. In Fig. 9(a), are provided the numerical results for the efficiency function as a function of U_θ/S_L for $0.4S_L \leq U_c - U^u(X_c) \leq 4.7S_L$. Noticeable is the non monotonic evolution of C with respect to U_θ/S_L that was previously observed in the experiments (see Fig. 4). Furthermore, one clearly observes a dependence

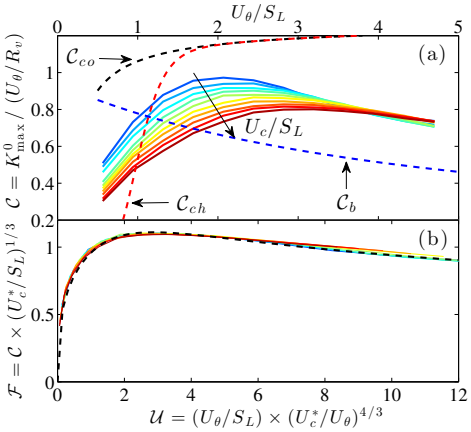

Figure 9: (a) Efficiency function as a function of U_θ/S_L for different values of U_c/S_L. Colours from blue to red indicate increasing value of U_c/S_L which varies between 0.4 and 4.7. (b) Rescaled efficiency function as a function of a rescaled velocity ratio. The black dashed line represent the fit using Eq. (4)

of C on U_c. Note that for $U_\theta/S_L > 3.5$ the effect of U_c is almost negligible. In Fig. 9(b), it is shown that the evolution of C with respect to U_c and U_θ can be represented by a single curve, when the rescaled efficiency function $\mathcal{F} = C \times (U^*_c/S_L)^{1/3}$ is plotted as a function of a rescaled velocity ratio $\mathcal{U} = (U_\theta/S_L)\times(U^*_c/U_\theta)^{4/3}$, where $U^*_c = U_c - U^u(X_c) + S_L$ is the relative velocity between the flame and the vortex centers [3]. This curve highlights a first zone for $U_\theta/S_L < 2.5$ where $\mathcal{F}$ scales as $\mathcal{U}^{1/3}$, and a second zone at larger U_θ/S_L for which $\mathcal{F}$ decreases as $\mathcal{U}^{-1/4}$. This trend can be well fitted by the following parametric expression (the black dashed line in Fig. 9(b))

$$\mathcal{F} = \mathcal{U}^{1/3}\left[1 + \left(\frac{\mathcal{U}}{\mathcal{U}_{\max}}\right)^2\right]^{\frac{-1/4-1/3}{2}}, \qquad (4)$$

from which $C = \mathcal{F} \times (U^*_c/S_L)^{-1/3}$ can be recovered. $\mathcal{U}_{\max}$ is the rescaled velocity ratio for which the bending of $\mathcal{F}$ is observed and was found to be equal to 2.5. The ability of this expression for modelling the flame stretch from the vortex strain is emphasized in Fig. 10. Departures between modelled and measured $K^0_{\max}$ are similar Fig. 8, i.e. within 20%. The present formulation for C further appears to be more adequate than either that of Colin et al. [6], Charlette et al. [7] or Bougrine et al. [8].

5. Conclusion

The present study is devoted to the exploration of the flame stretch induced by a vortex dipole with special emphasis on the *strain-sweeping competition*.

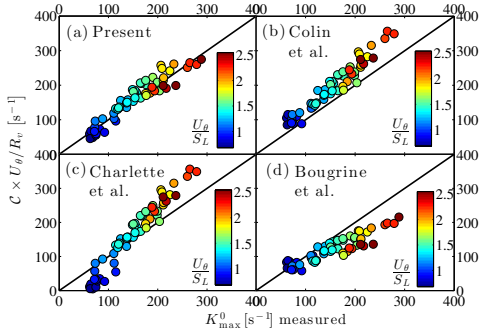

Figure 10: Scatter plot of the measured vs modelled flame stretch using the present efficiency function (a), that of Colin et al. [6] (b), Charlette et al. [7] (c) and Bougrine et al. [8] (d). Symbols are coloured by U_θ/S_L

Both experiments and numerical simulations of a stagnation flame have been carried out, with the aim of assessing the ability of available parametric expression for describing the efficiency function.

It was first shown that, though based on the same numerical data, C provided by both Colin et al. [6], Charlette et al. [7] predicts an increase of C with respect to U_θ/S_L whereas that of Bougrine et al. [8] emphasizes the opposite trend. In addition, they appear to depart quite significantly from experimental data and they fail in describing the non-monotonic evolution of C with respect to U_θ/S_L.

Secondly, by comparing experiments to simplified numerical simulations based on the 'isothermal' G-equation, it was shown that the early stage of interaction is driven by a kinematic interaction between the vortex the flame.

Finally, these simulations allow the effect of the residence time of the vortex in the vicinity of the flame to be investigated. A new parametric expression for the efficiency function is proposed and compares favourably well with experimental data. As mentioned in the introduction, in 'real' turbulent flows, a given scale r with characteristic velocity u_r has a strain characteristic time scale $\tau_s \propto r/u_r$ whilst the convection (or sweeping) characteristic time scale is These two distinct time scales are thus representative of rather small (u_r) and large scales (u') phenomena respectively. This indicates that in a LES, C can be evaluated using the sub-grid scale velocity for U_θ and the total (resolved + sub-grid scale) velocity for U_c.

Acknowledgements

The financial support from the Agence National de la Recherche under the project IDYLLE is gratefully acknowledged. We are also thankful to the CNRS, the University of Orléans, and the French Government Program "Investissements d'avenir" through the LABEX CAPRYSSES. FT acknowledges EADS for its financial support. We also benefited from the computing resources provided by CaSciModOT. We thank Laurent Catherine for his technical assistance.

References

[1] T. Poinsot, D. Veynante, S. Candel, J. Fluid Mech. 228 (1991) 561–606.

[2] W. L. Roberts, J. F. Driscoll, Combust. Flame 87 (1991) 245–256.

[3] M.-S. Wu, J. F. Driscoll, Combust. Flame 91 (1992) 310–322.

[4] W. L. Roberts, J. F. Driscoll, M. C. Drake, L. P. Goss, Combust. Flame 94 (1993) 58–69.

[5] T.-W. Lee, D. Santavicca, Combust. Sci. Technol. 90 (1993) 211–229.

[6] O. Colin, F. Ducros, D. Veynante, T. Poinsot, Phys. Fluids 12 (2000) 1843–1863.

[7] F. Charlette, C. Meneveau, D. Veynante, Combust. Flame 131 (2002) 159–180.

[8] S. Bougrine, S. Richard, O. Colin, D. Veynante, Flow, turbul. combust. 93 (2014) 259–281.

[9] J. F. Driscoll, Prog. Energ. Combust. 34 (2008) 91–134.

[10] A. Kolmogorov, Proc. USSR Ac. of Sci. 30 (1941) 299–303.

[11] H. Tennekes, J. Fluid Mech. 67 (1975) 561–567.

[12] C. Poulain, N. Mazellier, L. Chevillard, Y. Gagne, C. Baudet, Eur. Phys. J. B 53 (2006) 219–224.

[13] N. Bouvet, D. Davidenko, C. Chauveau, L. Pillier, Y. Yoon, Combust. Flame 161 (2014) 438–452.

[14] W. Thielicke, E. J. Stamhuis, Journal of Open Research Software 2 (2014) 30.

[15] R. Trieling, J. Van Wesenbeeck, G. Van Heijst, Phys. Fluids 10 (1998) 144–159.